

EFFICIENTIML: EFFICIENT HIGH-RESOLUTION IMAGE MANIPULATION LOCALIZATION

Jinhan Li¹, Haoyang He², Lei Xie², Jiangning Zhang²

¹ New York University, New York, NY, United States ² Zhejiang University, Hangzhou, China

ABSTRACT

With imaging devices delivering ever-higher resolutions and the emerging diffusion-based forgery methods, current detectors trained only on traditional datasets (with splicing, copy-moving and object removal forgeries) lack exposure to this new manipulation type. To address this, we propose a novel high-resolution SIF dataset of 1,200+ diffusion-generated manipulations with semantically extracted masks. However, this also imposes a challenge on existing methods, as they face significant computational resource constraints due to their prohibitive computational complexities. Therefore, we propose a novel EfficientIML model with a lightweight, three-stage EfficientRWKV backbone. EfficientRWKV’s hybrid state-space and attention network captures global context and local details in parallel, while a multi-scale supervision strategy enforces consistency across hierarchical predictions. Extensive evaluations on our dataset and standard benchmarks demonstrate that our approach outperforms ViT-based and other SOTA lightweight baselines in localization performance, FLOPs and inference speed, underscoring its suitability for real-time forensic applications.

Index Terms— Image Manipulation Localization, High Resolution Dataset, Lightweight RWKV

1. INTRODUCTION

Modern forensic analysis increasingly relies on Image Manipulation Localization (IML) to detect and precisely mask manipulated regions in digital images. With the development of high-fidelity diffusion-based inpainting methods such as Stable Diffusion[1] and the proliferation of ultra-high-resolution imaging devices, traditional localization techniques must now handle subtler manipulations over vastly larger canvases.

Numerous benchmark datasets have driven progress in image forgery localization, including CASIA V1/V2[2][3], Columbia[4], NIST16[5], DEFACTO[6], Coverage[7], IMD[8] and more recently, CIMD[9]. Despite their importance, these collections are largely composed of low/medium-resolution images and simple artifact-based manipulations, which constrain their utility for training detectors aimed at identifying semantic, diffusion-generated forgeries at the high resolutions that are common in current applications. Although diffusion-

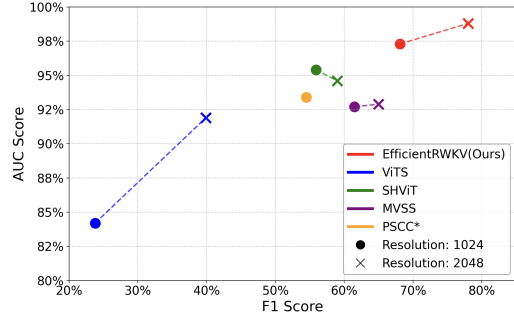


Fig. 1: Performance of SOTA Architectures on SIF dataset

based datasets such as CSI-IMD[10] have been proposed, their low resolution (below 600×800) prevents alignment with the operational scales of modern detectors.

To overcome these dataset gaps, we introduce the SIF (Semantic Inpainting Forgery) dataset, the first publicly released high-resolution semantic dataset exceeding 1024×1024. SIF comprises 1200+ carefully curated, diffusion-generated inpainted images at up to 1800×1200 resolution, all hand-picked and human-validated by our group members and volunteers for semantic correctness and visual quality.

At the same time, localizing subtle forgeries in large images remains a formidable challenge. Vision transformer (ViT)-based detectors (such as IML-ViT[11]) suffer from quadratic complexity, making them impractical for on-device or real-time analysis. On the other hand, many CNN models such as MVSS-Net[12] either sacrifice long-range context or incur similar prohibitive FLOPs when scaled to higher resolutions. Existing lightweight architectures such as SHViT[13] still demand over 380 GFLOPs at 2048×2048 inputs.

In this work, we address these limitations by proposing a novel EfficientRWKV backbone based on Vision-RWKV[14].

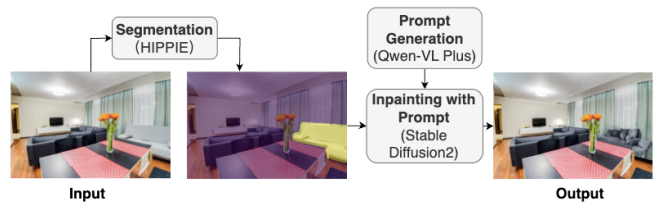


Fig. 2: Pipeline for Creating SIF Dataset

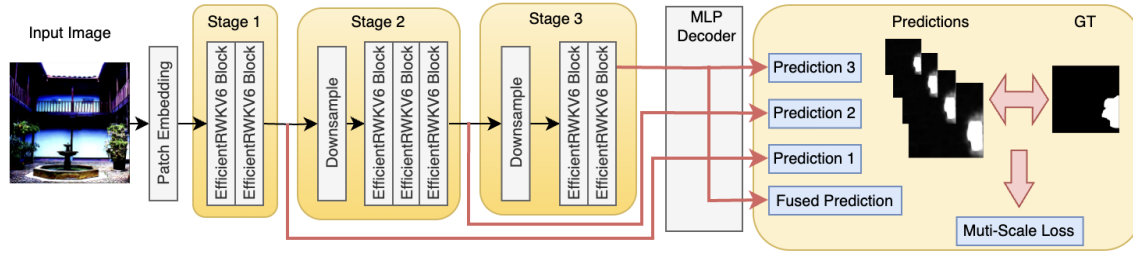


Fig. 3: Macro Design

It only requires a small fraction of the computational resources compared to the lightweight SOTA models, allowing it to operate on higher resolution datasets with limited computational resources. Even when input size grows to 2048×2048, we kept the computational cost under 100 GFLOPs. The primary contributions of this paper are:

1. **SIF dataset**, the first ultra-high-resolution semantic inpainting forgery dataset beyond 1024×1024.
2. A lightweight, three-stage **EfficientRWKV** backbone that fuses global state-space attention and local convolutional processing, with linear computational complexities.
3. A multi-scale decoder equipped with tailored loss weights.

2. HIGH-RESOLUTION SIF DATASET

In this study, we introduce a high-resolution manipulated image dataset consisting of 1,228 carefully curated samples. Our construction pipeline is a modified version based on the Inpaint Anything framework[15] and the source images are selected from the SAM9K dataset[16]. The procedure for dataset generation is illustrated in Fig. 2.

For an input image, we leverage the Hierarchical Open-vocabulary Universal Image Segmentation[17] (HIPPIE) to segment for the object mask, and use a vision-language model, Qwen-VL Plus[18], to generate an appropriate prompt for inpainting. Then, the prompt, original image, and mask are input into Stable Diffusion 2 [1]. This model replaces the masked region in the image with semantically coherent and visually consistent content, guided by the prompt. The result is a manipulated image that maintains high visual fidelity while incorporating subtle or significant alterations.

Approximately 5,000 manipulated images were generated through the above pipeline. From this pool, a final set of 1,228 images was manually selected based on visual realism, semantic coherence, and diversity of manipulations.

3. METHODOLOGY: EFFICIENTIML

In this work, we propose a novel and efficient image manipulation localization framework EfficientIML (Fig. 3) by integrating an optimized EfficientRWKV backbone with a customized multi-scale prediction scheme. Our pipeline

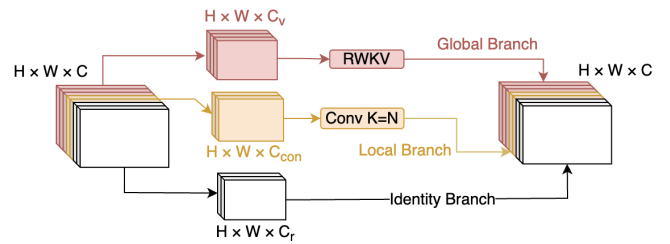


Fig. 4: EfficientRWKV6 Module

builds upon the baseline structure of IML-ViT[11], but introduces these two significant architectural innovations to improve both performance and efficiency.

3.1. EfficientRWKV Backbone

We develop a lightweight attention backbone called **EfficientRWKV**, based on Vision RWKV6[14], made up of multiple EfficientRWKV blocks. It incorporates multi-scale embedding, stage-wise attention, and adaptive downsampling.

EfficientRWKV Block. This block is a lightweight yet expressive building unit designed to capture both global and local visual dependencies while maintaining efficiency. Each EfficientRWKV Block consists of a sequential application of the following components, including depthwise convolution residual modules, a token mixer implemented via the EfficientRWKV Module, and Point-wise Feed Forward Networks (FFNs). Among them, the EfficientRWKV Module (Fig. 4) performs multi-branch attention. It splits the input tensor x along the channel dimension into three specialized branches: **Global Branch** (x_g): A fixed number of channels (C_v) is allocated to the global branch, which captures long-range dependencies via the recurrent-style attention mechanism of Vision-RWKV6 [14], enabling efficient, context-aware representation learning without explicit pairwise attention.

Local Branch (x_l): A second group of channels (C_{con}) is passed through a depthwise separable convolutional block to capture fine-grained, local spatial patterns. The kernel size(K) of the block varies with the stage number.

Identity Branch (x_i): The remaining channels bypass both global and local processing, preserving raw input features.

Table 1: CASIAV2-training with resolution 1024×1024

(a) Pixel-level F1 Score (%)								(b) AUC Score (%)							
	CASIAV1	Columbia	Coverage	NIST16	IMD	CIMD	Average		CASIAV1	Columbia	Coverage	NIST16	IMD	CIMD	Average
ViT-S[11]	32.7	24.1	4.8	15.7	19.3	9.8	17.7	ViT-S	78.6	68.3	62.8	70.1	74.1	75.7	71.6
SHViT[13]	49.7	79.1	36.3	20.0	27.4	17.5	38.3	SHViT	85.5	92.5	85.1	74.6	77.4	79.7	82.4
MVSS[12]	41.9	57.3	34.5	21.2	30.9	17.4	33.9	MVSS	81.6	84.2	83.5	70.8	78.9	71.3	78.4
PSCC ⁺ [19]	44.5	62.5	19.4	19.8	31.0	6.0	30.5	PSCC ⁺	77.3	82.8	79.0	69.6	81.6	66.0	76.1
Ours	60.9	76.6	38.6	24.2	32.4	23.12	42.6	Ours	90.6	87.9	82.4	76.2	80.1	81.8	83.2

(c) IoU Score (%)								(d) Accuracy Score (%)							
	CASIAV1	Columbia	Coverage	NIST16	IMD	CIMD	Average		CASIAV1	Columbia	COVERAGE	NIST16	IMD	CIMD	Average
ViT-S	26.3	15.8	2.5	10.7	13.8	6.7	12.6	ViT-S	91.2	74.4	87.2	89.7	91.3	97.5	88.5
SHViT	45.1	69.4	31.1	15.9	21.8	13.4	32.8	SHViT	93.6	89.9	91.6	89.7	92.8	98.1	92.6
MVSS	37.0	46.5	26.5	16.2	24.0	13.5	27.3	MVSS	94.4	83.2	90.1	90.8	92.5	96.4	91.2
PSCC ⁺	37.2	50.7	13.3	14.5	23.2	3.8	23.8	PSCC ⁺	79.4	76.1	86.6	79.1	89.1	75.4	80.9
Ours	56.6	69.0	36.2	20.1	27.1	19.0	38.0	Ours	95.8	86.9	91.9	92.6	93.0	97.9	93.0

This facilitates gradient flow through shortcut connections and reduces channel redundancy in high-dimensional space. **Macro Backbone Design.** This is shown in Fig. 3. For an input image $X \in \mathbb{R}^{H \times W \times 3}$, it is embedded into a $(\frac{H}{16}, \frac{W}{16}, C_1)$ feature map, fed into the first stage of EfficientRWKV backbone. Each stage of the backbone includes progressive down-sampling through Patch Merging and residual Feed-Forward Network (FFN) blocks to maintain rich multi-scale spatial features. Feature maps processed in stage 2 and 3 are $(\frac{H}{32}, \frac{W}{32}, C_2)$ and $(\frac{H}{64}, \frac{W}{64}, C_3)$ respectively. Due to the decrease from quadratic complexity to linear complexity in the foundational attention architectures, the window-based attention strategy in IML-ViT[11] is no longer necessary.

The output of the three backbone stages yields three feature maps that progressively reduce spatial resolution.

3.2. Multi-Scale Decoder with Loss Supervision

The multi-scale features are then passed to a multi-branch decoder head. The decoder outputs the fused prediction as well as intermediate predictions at each resolution. Using multi-scale features directly from different stages of the backbone offers several advantages over extracting only the final feature and relying on a separate Simple Feature Pyramid Network (as done in IML-ViT[11]). First, the features at early stages inherently preserve finer spatial details and shallow representations. Second, this direct multi-stage integration enables more efficient gradient flow, which improves learning stability and accelerates convergence. Lastly, it reduces computational overhead by eliminating the need for a separate SFPN.

The total training loss $\mathcal{L}_{\text{total}}$ consists of edge-aware supervision from IML-ViT[11] and multi-scale prediction loss.

$$\mathcal{L}_{\text{total}} = \sum_{i=1}^3 \lambda_i \cdot \text{BCE}(\hat{M}_i, M_i) + \lambda_{\text{edge}} \cdot \sum_{i=1}^3 \text{BCE}(\hat{M}_i, M_i; E_i) + \lambda \cdot \text{BCE}(\hat{M}_{\text{final}}, M) + \lambda_{\text{edge}} \cdot \text{BCE}(\hat{M}_{\text{final}}, M; E)$$

In the above formula, \hat{M}_i denotes the predicted mask at

the i -th intermediate resolution. M_i is the ground-truth mask downsampled to the same resolution as \hat{M}_i . E_i is the corresponding edge mask and \hat{M}_{final} is the upsampled final prediction. M and E are the ground-truth full-resolution mask and edge map, respectively. λ_i are the weights for multi-scale prediction losses. λ_{edge} is the edge loss hyperparameter.

4. EXPERIMENT

4.1. Implementation Details

EfficientRWKV. The EfficientRWKV backbone uses a pre-trained checkpoint obtained by pre-training for 1,000 epochs on ImageNet-1K under a teacher–student distillation regime, with a TResNet-L network[20] providing soft targets according to the DeiT distillation protocol[21]. Training is performed with an effective batch size of 64, using the AdamW[22] optimizer with an initial learning rate of 1×10^{-4} and a cosine decay schedule[23].

ViT-S. The vision transformer in IML-ViT[11] method is modified to be ViT-S, a lighter version of ViT with checkpoint ViT-S/16 from DINO[24], to ensure fairness in comparison.

SHViT. We also replace the attention module in IML-ViT[11] with SHViT-S4[13], by Yun and Ro et al.

MVSS[12] & PSCC[19]. We employ IMDL-BenCo[25], a comprehensive platform for IMDL tasks, to experiment on these two models. PSCC has 512×512 instead of 1024×1024 inputs due to its high demand for GPU memory.

Training/Testing Dataset.

- CASIAV2-training: Aligning with IML-ViT[11], we use entire CASIAV2 for training, other datasets for testing.
- SIF-training: In the second experiment, SIF dataset is split with a 6:1 ratio for training and testing.

Evaluation Criteria. We evaluate all models using four metrics: Pixel-F1 score, Area Under the ROC Curve (AUC), Intersection over Union (IoU), and Pixel-Accuracy.

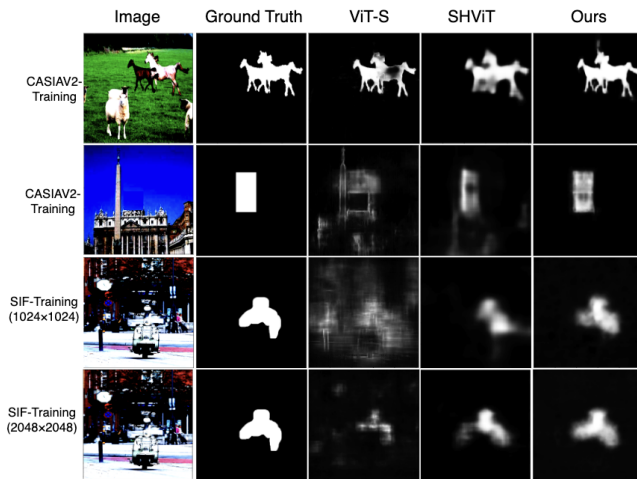
Table 2: SIF-training at different resolutions

(a) Resolution 1024×1024(%)					(b) Resolution 2048×2048(%)				
	F1	AUC	IoU	ACC		F1	AUC	IoU	ACC
ViT-S	23.8	84.2	16.9	95.1	ViT-S	39.9	91.9	29.2	96.3
SHViT	55.9	95.4	43.9	96.9	SHViT	59.0	94.6	47.6	97.1
MVSS	61.5	92.7	48.5	96.9	MVSS	65.0	92.9	51.3	97.1
PSCC	54.5	93.4	41.5	95.2	PSCC	-	-	-	-
Ours	68.1	97.3	56.2	97.4	Ours	78.0	98.8	67.3	98.2

4.2. Comparison with SoTAs

Quantitative Results. Under the CASIAV2-training protocol (Tab. 1), our model has consistently strong performance across all metrics. For F1 and IoU, it has increased performance of +4.3% and +5.2% over the best SOTA model tested.

Tab. 2b presents the evaluation results on the SIF dataset trained and tested at resolution of 2048×2048. Our proposed model again demonstrates clear superiority across all four metrics, with a +13% difference compared to the best model. This increase confirms the effectiveness of our architecture in capturing fine-grained manipulations in large images.

**Fig. 5: Qualitative Comparison**

Qualitative Results. The qualitative comparison shown in Fig. 5 highlights the validity of our proposed model across both CASIAV2-trained and SIF-trained settings. In the first two rows (CASIAV2-training), our method shows significantly more accurate localization than ViT-S and sharper predictions than SHViT[13]. In the bottom row with higher resolution, our model leverages the additional details, becoming noticeably better aligned with ground truth.

Efficiency. As shown in Tab. 3, our method achieves a superior computation-throughput trade-off among state-of-the-art approaches. At 1024×1024 resolution, it requires only approximately **22.7%** of the computational resources as SHViT[13] (lightest model tested) used and around **3.3%** as the SOTA model MVSS[12] used. With ultra-high resolution at around 2048×2048, our model incurs just 86.7

Table 3: Model Complexity (*: Checkpointing used)

	Params(M)	1024×1024		2048×2048	
		GFLOPS	Speed(img/s)	GFLOPS	Speed(img/s)
ViT-S	22.6	128.2	37.8	512.7*	9.3*
SHViT	19.5	95.6	71.7	382.4	16.9
MVSS	142.8	654.3	11.0	2617.8	2.4
PSCC	3.7	116.2	13.8	-	-
Ours	19.8	21.7	58.5	86.7	23.0

GFLOPs, still maintaining the usage of around **22.7%** of the computational resources as the lightest comparison model.

Table 4: Model Ablation Studies

*: See Appendix Table 8

	F1	AUC	IoU	ACC
Loss Weights Set 1 *	65.7	97.1	54.1	97.3
Loss Weights Set 2 *	65.2	96.9	53.6	97.2
Loss Weights Set 3 *	65.8	97.0	54.6	97.4
Pretrained w/o Knowledge Distillation	63.8	96.5	52.9	97.4
Freeze Global Branch Weights	57.3	96.8	46.3	96.8
Freeze Local Branch Weights	64.2	97.0	53.0	97.2
Final Setup	68.1	97.3	56.2	97.4

4.3. Ablation

Multi-Loss Weights. We tested other sets of loss weight and our chosen set achieves the best result (Tab. 4).

Pre-training. Two pretrained checkpoints are tested: One is pretrained with knowledge distillation and the other without. Employing this special pre-training technique boosts our model performance by 4.3% in F1.

Ablation on EfficientRWKV. According to Tab. 5 row 1 and 2, EfficientRWKV is proven to be a more effective replacement of ViT-S. We also conducted two ablation trials to validate the effectiveness of the branches in EfficientRWKV.

Table 5: Model Incremental Ablation Studies

Backbone	SFPN	Multi-S Loss	F1	AUC	IoU	ACC
ViT-S	Yes	No	23.8	84.2	16.9	95.1
Effi-RWKV	Yes	No	57.6	97.1	47.0	97.1
Effi-RWKV	No	No	61.6	95.5	50.0	97.0
Ours	No	Yes	68.1	97.2	56.2	97.4

5. CONCLUSION

In this paper, we introduce SIF, the first high-resolution semantic inpainting forgery dataset and EfficientIML with a lightweight three-stage backbone of linear complexity and a multi-scale decoder under hierarchical loss supervision. Extensive experiments on SIF and standard benchmarks demonstrate that our method achieves state-of-the-art localization performance and runtime efficiency.

Appendix

A. SIF DATASET RELATED

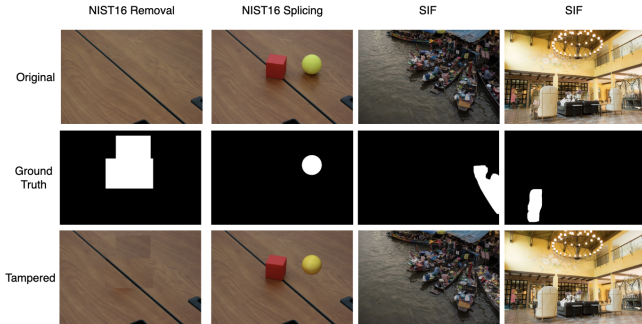


Fig. 6: Comparison between SIF and NIST16

Fig. 6 highlights a qualitative difference between NIST16 (an existing and widely-used high-resolution dataset) and our SIF dataset. In NIST16 (left two columns), manipulated regions are restricted to simple geometric primitives that sometimes bear little relation to image content. By contrast, SIF’s context-aware masks trace the contours of actual scene elements, so the inpainted areas correspond to semantically meaningful objects (e.g. furniture or vessels). This context-aware masking is far more closely aligned with real-world scenarios, producing highly realistic forgeries and yielding a far more effective and valuable training dataset for high-resolution localization methods.

Table 6: Current IML Datasets / SIF Dataset

Dataset	# Manipulated Images	Resolution
CASIA V1[2]	921	~384×256
CASIA V2[3]	5,123	384×256 to 800×600
Columbia[4]	180	757×568 to 1152×768
NIST16[5]	564	Up to 3744×5616
DEFACTO[6]	229,000	~640×480
COVERAGE[7]	100	235×158 to 752×563
ForenSynths[26]	100,000	256×256
CSI-IMD[10]	1000	400×296 to 600×800
SIF	1,228	~1800×1200

B. EFFICIENTRWKV RELATED

B.1. Additional Details about Model

The three channel sizes used in each stage are [$C_1 = 200$, $C_2 = 376$, $C_3 = 448$].

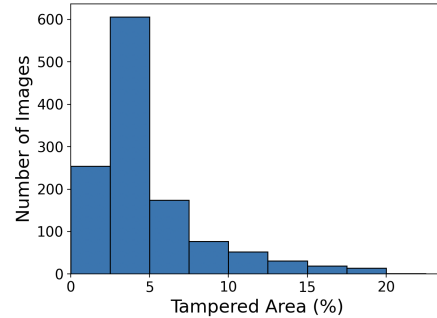


Fig. 7: Tampered Region Ratio of SIF

Table 7: Channel Allocation per Stage

Stage	C_v	C_{con}	C_i
1	$0.8 \times C$	$0.2 \times C$	$0 \times C$
2	$0.7 \times C$	$0.2 \times C$	$0.1 \times C$
3	$0.6 \times C$	$0.3 \times C$	$0.1 \times C$

B.2. Additional Details about Ablation Experiments

Tab. 8 contains the details of the three loss weight sets used in ablation studies. Our chosen weighting scheme achieves the best performance, delivering an approximately 2.5% improvement in F1 score over other configurations. These findings indicate that more emphasis should be given to the deeper layers, although taking multi-scale loss benefits the performance of the model.

Table 8: Weights for Model Outputs in Ablation Studies

Set Number	Layer 1	Layer 2	Layer 3	Fused Output
Loss Weights Set 1	0.25	0.35	0.45	1.0
Loss Weights Set 2	0.35	0.35	0.35	1.0
Loss Weights Set 3	0.5	0.5	0.5	0.5
Final Setup	0.15	0.35	0.55	1.0

For local/global branch studies, we also include a qualitative result to show the difference in Fig. 8, corresponding to the decreased value in testing metrics. When the global branch is frozen, the predicted mask lacks confidence and exhibits excessively blurred boundaries; moreover, false positives appear to the right of the whole prediction. Conversely, freezing the local branch yields a mask with a highly confident predicted area, also accompanied by false positives towards the right. Only when both branches operate together does the model reconcile coarse, context-driven localization with fine, edge-aware refinement, eliminating the majority of

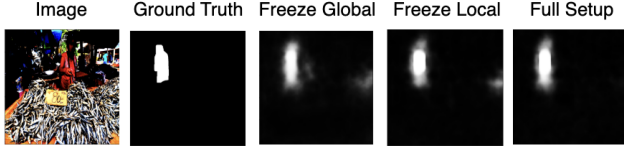


Fig. 8: Full Set up and freezing Local/Global Branches

false positives and producing a sharply delineated mask that faithfully matches the ground truth.

C. RWKV BASICS

Our global attention branch is based on RWKV. Specifically, the Bi-WKV module computes global attention as:

$$\text{wkv}_t = \frac{\sum_{i=0, i \neq t}^{T-1} \exp\left(-\frac{|t-i|-1}{T}w + k_i\right) v_i + \exp(u + k_t) v_t}{\sum_{i=0, i \neq t}^{T-1} \exp\left(-\frac{|t-i|-1}{T}w + k_i\right) + \exp(u + k_t)}$$

WKV recurrence[14] is used here in Equation (1). $w, u \in \mathbb{R}^{C_v}$ are learnable channel-wise decay and bias vectors, and k_i, v_i are the key/value features at position i , yielding $\mathcal{O}(TC_v)$ complexity.

D. RELATED WORK

D.1. Image Forgery Dataset

Conventional image forgery techniques primarily involve copy-move, splicing, and object removal. Accordingly, many image forgery detection datasets are constructed following these manipulation types, including CASIA V1/V2[2][3], Columbia[4], NIST16[5], DEFACTO[6], and Coverage[7]. Recent deep learning-generated datasets such as ForenSynths[26] have trivial and unified artifacts that are often easier to detect, as their creator notices. On the other hand, our proposed dataset employs Stable Diffusion[1] for inpainting, attempting to model the challenge of detecting more subtle AI-generated traces. Moreover, most existing image forgery datasets consist predominantly of low/medium-resolution images, which may not adequately represent the quality of manipulations generated by modern generative models and advanced editing tools. For instance, the CASIA v2.0 dataset contains images with average resolutions below 500×500 , and the Columbia dataset typically features images below 1000×1000 pixels. In this work, we introduce a dataset comprising images with resolutions around 1800×1200 , thereby providing a more suitable benchmark for evaluating image forgery localization models under high-resolution settings.

D.2. CNN Based Image Forgery Localization

Before the rise of Vision Transformers, Convolutional Neural Networks (CNNs) were the dominant architecture for the

task of image manipulation localization. Early approaches like ManTra-Net[27] focused on learning local artifact features through an encoder-decoder framework that combines manipulation traces and classification clues. PSCC-Net[19] advanced this by introducing a pyramid structure and spatial-channel correlation modules to capture multi-scale inconsistencies. MVSS-Net[12] has further improved performance by integrating both RGB content and noise streams, guided by edge supervision, to highlight manipulation boundaries. These CNN-based methods laid the groundwork for spatially aware manipulation localization, but often struggled with capturing relatively long-range dependencies and generalizing across diverse manipulation types.

D.3. ViT Based Image Forgery Localization

Significant advancements in image manipulation localization are made possible by leveraging the power of Vision Transformer. Omni-IML[28] presents a unified framework capable of localizing a wide range of manipulation types. However, the use of large-scale ViT backbones leads to substantial computational costs. Similarly, IML-ViT[11] (which serves as our baseline), along with other ViT-based models, faces scalability challenges, particularly when processing high-resolution images, due to their high computational complexity and memory consumption. With the demand for processing images with higher resolutions, significant efforts are made to reduce model complexity, such as token pruning presented by EvoViT[29], or window-based attention layers in IML-ViT[11]. However, these techniques tend to have limited effects as opposed to strategies that directly modify the model’s backbone architecture.

E. REFERENCES

- [1] Robin Rombach, Andreas Blattmann, Dominik Lorenz, Patrick Esser, and Björn Ommer, “High-resolution image synthesis with latent diffusion models,” 2021.
- [2] Jing Dong, Wei Wang, and Tieniu Tan, “CASIA image tampering detection evaluation database,” in *2013 IEEE China Summit and International Conference on Signal and Information Processing*. July 2013, IEEE.
- [3] Nam Thanh Pham, Jong-Weon Lee, Goo-Rak Kwon, and Chun-Su Park, “Hybrid image-retrieval method for image-splicing validation,” *Symmetry*, vol. 11, no. 1, pp. 83, 2019.
- [4] Y.-F. Hsu and S.-F. Chang, “Detecting image splicing using geometry invariants and camera characteristics consistency,” in *International Conference on Multimedia and Expo*, 2006.
- [5] Haiying Guan, Mark Kozak, Eric Robertson, Yooyoung Lee, Amy Yates, Andrew Delgado, Daniel Zhou, Timothée Kheyrkhan, Jeff Smith, and Jonathan, “Mfc datasets: Large-scale benchmark datasets for media forensic challenge evaluation,” in *Conference Proceedings*. 2019-01-11 00:01:00 2019, IEEE Winter Conference on Applications of Computer Vision (WACV 2019), Waikola, HI.
- [6] Gaël Mahfoudi, Badr Tajini, Florent Retraint, Fr’ed’eric Morain-Nicolier, Jean Luc Dugelay, and Marc Pic”, “DEFACTO: image and face manipulation dataset,” in *27th European Signal Processing Conference (EUSIPCO 2019)*, A Coruña, Spain”, sep 2019.
- [7] Bihan Wen, Ye Zhu, Ramanathan Subramanian, Tian-Tsong Ng, Xuanjing Shen, and Stefan Winkler, “Coverage – a novel database for copy-move forgery detection,” in *IEEE International Conference on Image processing (ICIP)*, 2016, pp. 161–165.
- [8] Adam Novozamsky, Babak Mahdian, and Stanislav Saic, “Imd2020: A large-scale annotated dataset tailored for detecting manipulated images,” in *2020 IEEE Winter Applications of Computer Vision Workshops (WACVW)*, March 2020, pp. 71–80.
- [9] Zhenfei Zhang, Mingyang Li, and Ming-Ching Chang, “A new benchmark and model for challenging image manipulation detection,” *Proceedings of the AAAI Conference on Artificial Intelligence*, vol. 38, no. 7, pp. 7405–7413, Mar. 2024.
- [10] Yuwei Chen, Ming-Ching Chang, Mattias Kirchner, Zhenfei Zhang, Xin Li, Arslan Basharat, and Anthony Hoogs, “A Semantically Impactful Image Manipulation Dataset: Characterizing Image Manipulations Using Semantic Significance,” in *2025 IEEE/CVF Winter Conference on Applications of Computer Vision (WACV)*, Los Alamitos, CA, USA, Mar. 2025, pp. 7659–7668, IEEE Computer Society.
- [11] Xiaochen Ma, Bo Du, Zhuohang Jiang, Ahmed Y. Al Hammadi, and Jizhe Zhou, “Iml-vit: Benchmarking image manipulation localization by vision transformer,” 2023.
- [12] Chengbo Dong, Xinru Chen, Ruohan Hu, Juan Cao, and Xirong Li, “Mvss-net: Multi-view multi-scale supervised networks for image manipulation detection,” *IEEE Transactions on Pattern Analysis and Machine Intelligence*, pp. 1–14, 2022.
- [13] Seokju Yun and Youngmin Ro, “Shvit: Single-head vision transformer with memory efficient macro design,” in *Proceedings of the IEEE/CVF Conference on Computer Vision and Pattern Recognition (CVPR)*, 2024, pp. 5756–5767.
- [14] Yuchen Duan, Weiyun Wang, Zhe Chen, Xizhou Zhu, Lewei Lu, Tong Lu, Yu Qiao, Hongsheng Li, Jifeng Dai, and Wenhai Wang, “Vision-rwkv: Efficient and scalable visual perception with rwkv-like architectures,” *arXiv preprint arXiv:2403.02308*, 2024.
- [15] Tao Yu, Runseng Feng, Ruoyu Feng, Jinming Liu, Xin Jin, Wenjun Zeng, and Zhibo Chen, “Inpaint anything: Segment anything meets image inpainting,” *arXiv preprint arXiv:2304.06790*, 2023.
- [16] Lin Chen, Jinsong Li, Xiaoyi Dong, Pan Zhang, Conghui He, Jiaqi Wang, Feng Zhao, and Dahua Lin, “Sharegpt4v: Improving large multi-modal models with better captions,” in *European Conference on Computer Vision*. Springer, 2024, pp. 370–387.
- [17] Xudong Wang, Shufan Li, Konstantinos Kallidromitis, Yusuke Kato, Kazuki Kozuka, and Trevor Darrell, “Hierarchical open-vocabulary universal image segmentation,” in *Thirty-seventh Conference on Neural Information Processing Systems*, 2023.
- [18] Jinze Bai, Shuai Bai, Shusheng Yang, Shijie Wang, Sinan Tan, Peng Wang, Junyang Lin, Chang Zhou, and Jingren Zhou, “Qwen-vl: A versatile vision-language model for understanding, localization, text reading, and beyond,” *arXiv preprint arXiv:2308.12966*, 2023.
- [19] Xiaohong Liu, Yaojie Liu, Jun Chen, and Xiaoming Liu, “Psc-net: Progressive spatio-channel correlation network for image manipulation detection and localization,” *IEEE Transactions on Circuits and Systems for Video Technology*, 2022.
- [20] Tal Ridnik, Hussam Lawen, Asaf Noy, Emanuel Ben Baruch, Gilad Sharir, and Itamar Friedman, “Tresnet: High performance gpu-dedicated architecture,” 2020.
- [21] Hugo Touvron, Matthieu Cord, Matthijs Douze, Francisco Massa, Alexandre Sablayrolles, and Hervé Jégou, “Training data-efficient image transformers & distillation through attention,” 2021.
- [22] Ilya Loshchilov and Frank Hutter, “Decoupled weight decay regularization,” 2019.
- [23] Ilya Loshchilov and Frank Hutter, “Sgdr: Stochastic gradient descent with warm restarts,” 2017.
- [24] Mathilde Caron, Hugo Touvron, Ishan Misra, Hervé Jégou, Julien Mairal, Piotr Bojanowski, and Armand Joulin, “Emerging properties in self-supervised vision transformers,” in *Proceedings of the International Conference on Computer Vision (ICCV)*, 2021.
- [25] Xiaochen Ma, Xuekang Zhu, Lei Su, Bo Du, Zhuohang Jiang, Bingkui Tong, Zeyu Lei, Xinyu Yang, Chi-Man Pun, Jiancheng Lv, et al., “Imdl-benco: A comprehensive benchmark and codebase for image manipulation detection & localization,” *Advances in Neural Information Processing Systems*, vol. 37, pp. 134591–134613, 2025.
- [26] Sheng-Yu Wang, Oliver Wang, Richard Zhang, Andrew Owens, and Alexei A Efros, “Cnn-generated images are surprisingly easy to spot...for now,” in *CVPR*, 2020.
- [27] Yue Wu, Wael AbdAlmageed, and Premkumar Natarajan, “Mantra-net: Manipulation tracing network for detection and localization of image forgeries with anomalous features,” in *2019 IEEE/CVF Conference on Computer Vision and Pattern Recognition (CVPR)*, 2019, pp. 9535–9544.
- [28] Chenfan Qu, Yiwu Zhong, Fengjun Guo, and Lianwen Jin, “Omni-impl: Towards unified image manipulation localization,” 2024.
- [29] Yifan Xu, Zhijie Zhang, Mengdan Zhang, Kekai Sheng, Ke Li, Weiming Dong, Liqing Zhang, Changsheng Xu, and Xing Sun, “Evo-vit: Slow-fast token evolution for dynamic vision transformer,” in *Proceedings of the AAAI Conference on Artificial Intelligence*, 2022, vol. 36, pp. 2964–2972.